

Thermodynamic Properties of the Dunkl-Pauli Oscillator in an Aharonov-Bohm Flux

Ahmed Tedjani ^{1*}

Boubakeur Khantoul ^{1,2†}

¹Department of Process Engineering, University of Constantine 3 -Salah Boubnider, 25016 Constantine, Algeria

²Theoretical Physics Laboratory, Department of Physics, University of Jijel, Algeria

March 11, 2026

Abstract

We investigate the thermodynamic properties of a spin- $\frac{1}{2}$ particle described by the Dunkl-deformed Pauli equation in two dimensions in the presence of an Aharonov–Bohm (AB) flux. By replacing the standard momentum operators with Dunkl operators, the Hamiltonian incorporates reflection symmetry together with topological gauge effects. The magnetic flux imposes symmetry constraints on the Dunkl parameters, $\nu_1 + \varepsilon\nu_2 = 0$, linking the reflection sectors ($\varepsilon = \pm 1$) to the structure of the energy spectrum. Using the exact spectrum, we construct the canonical partition function and derive the thermodynamic quantities including the internal energy, entropy, and heat capacity. The results show that the interplay between Dunkl reflection symmetry and the AB phase leads to distinctive thermal behavior. In particular, the heat capacity exhibits a Schottky-type anomaly controlled by the magnetic flux, while at high temperatures the system approaches the classical oscillator limit.

1 Introduction

The study of low-dimensional quantum systems has revealed a wide range of phenomena that have no classical analogue, particularly when topology and symmetry play a central role [1, 2]. In two spatial dimensions, the interaction between charged particles and gauge fields leads to effects that depend not only on local forces but also on global properties of the configuration space. A paradigmatic example is the Aharonov–Bohm (AB) effect, in which a magnetic flux confined to an inaccessible region modifies the quantum phase of a particle moving in a field-free domain [3–6]. This phenomenon demonstrates that the vector potential has direct physical significance and influences measurable quantities such as the energy spectrum and interference patterns, as confirmed experimentally by Chambers [7] and Tonomura *et al.* [8]. The AB effect is closely related to geometric phases and gauge invariance [9] and continues to play an important role in modern quantum theory.

*Email: ahmed.tedjani@univ-constantine3.dz

†Email: boubakeur.khantoul@univ-constantine3.dz

For particles with spin, the appropriate framework is provided by the Pauli Hamiltonian [10], which describes the coupling between the intrinsic magnetic moment and an external electromagnetic field. As the non-relativistic limit of the Dirac equation [11], the Pauli equation captures important physical phenomena such as spin precession and the Zeeman interaction. In two-dimensional geometries, the combined action of spin interactions and magnetic flux leads to nontrivial spectral structures, particularly when boundary conditions and rotational symmetry are taken into account [12]. Such systems are relevant in mesoscopic physics and quantum nanostructures, including quantum rings and two-dimensional electron gases, where topological phases can be experimentally observed [13–15]. The Pauli equation in the presence of an AB flux has therefore been widely studied in various contexts [16, 17].

Beyond conventional quantum mechanics, deformations based on Dunkl operators have attracted considerable interest in mathematical physics. Introduced by Dunkl [18, 19] and further developed in subsequent works [20–22], these operators incorporate reflection symmetries directly into differential operators. As a result, the kinetic term of the Hamiltonian contains discrete reflection operators characterized by deformation parameters. Dunkl operators are closely related to integrable many-body systems such as the Calogero–Moser model [23–26], and they lead to modified angular momentum structures and generalized oscillator spectra. The Dunkl formalism has been applied to a variety of quantum systems, including Dirac and Klein–Gordon equations with Dunkl derivatives [27, 28], Dunkl–Pauli systems in magnetic fields [17, 29], and noncommutative phase-space extensions [30]. In these models, the presence of reflection symmetry introduces additional quantum sectors and modifies the structure of the energy spectrum.

When the Dunkl deformation is combined with an Aharonov–Bohm flux in two dimensions, the resulting model exhibits a rich interplay between discrete reflection symmetry and topological gauge phases. The magnetic flux shifts the angular momentum quantum number, while the Dunkl parameters modify the effective centrifugal potential, producing a deformed spectrum that reflects both topological and symmetry effects [17, 31, 32]. Such systems provide a useful theoretical framework for exploring the role of discrete symmetries and gauge fields in deformed quantum mechanics.

In the present work, we investigate the stationary Dunkl–Pauli equation in two dimensions in the presence of an Aharonov–Bohm flux. This study complements our previous analysis of the time-dependent case [33] by focusing instead on stationary states and their thermodynamic implications. After deriving the exact energy spectrum of the system, which reveals a topological constraint linking the Dunkl parameters to the reflection parity, we construct the canonical partition function and analyze the resulting thermodynamic quantities, including the internal energy, entropy, and heat capacity. Our results demonstrate how the combined effects of Dunkl reflection symmetry and the AB topological phase manifest in the statistical properties of the system, providing new insight into the thermodynamics of deformed quantum models in the presence of gauge fields.

2 Dunkl–Pauli Hamiltonian with Aharonov–Bohm Flux

We consider a spin- $\frac{1}{2}$ particle confined to the (x, y) plane and subjected to a static harmonic oscillator potential in the presence of a magnetic field. Its stationary states are governed by the time-independent Pauli equation

$$\left[\frac{1}{2M} (\boldsymbol{\sigma} \cdot \boldsymbol{\pi})^2 - \frac{eB(r)}{2M} \sigma_z + \frac{1}{2} M \omega^2 (x^2 + y^2) \right] \psi(x, y) = E \psi(x, y), \quad (1)$$

where $\boldsymbol{\sigma} = (\sigma_x, \sigma_y, \sigma_z)$ are the Pauli matrices and $\boldsymbol{\pi} = \mathbf{p} - e\mathbf{A}$ denotes the gauge-invariant momentum operator,

$$\boldsymbol{\pi} = (p_x - eA_x, p_y - eA_y), \quad (2)$$

with e the particle charge and natural units $c = \hbar = 1$. The two-component spinor wave function is written as $\psi = (\psi_1, \psi_2)^T$.

2.1 Aharonov–Bohm Configuration

To incorporate the Aharonov–Bohm (AB) effect [3, 4], we consider a magnetic flux ϑ confined to an infinitely thin solenoid along the z -axis. The magnetic field is singular at the origin,

$$e\mathbf{B}(r) = \frac{\vartheta}{r}\delta(r), \quad (3)$$

and in the Coulomb gauge the associated vector potential takes the azimuthal form

$$e\mathbf{A} = -\frac{\vartheta}{r}\mathbf{u}_\varphi = \frac{\vartheta y}{x^2 + y^2}\mathbf{i} - \frac{\vartheta x}{x^2 + y^2}\mathbf{j}. \quad (4)$$

2.2 Dunkl Deformation of the Momentum Operator

The Dunkl formalism introduces reflection operators into the kinetic structure [18, 19]. We replace the canonical momentum by the Dunkl momentum operator

$$p_j = \frac{1}{i}D_j, \quad D_j = \frac{\partial}{\partial x_j} + \frac{\nu_j}{x_j}(1 - R_j), \quad (5)$$

where $\nu_j > -\frac{1}{2}$ are real deformation parameters and R_j are reflection operators acting as $R_j f(x) = f(\dots, -x_j, \dots)$ with $R_j^2 = 1$. The Dunkl Laplacian follows as

$$\Delta_D = \sum_{j=1}^2 D_j^2 = \sum_{j=1}^2 \left(\frac{\partial^2}{\partial x_j^2} + \frac{2\nu_j}{x_j} \frac{\partial}{\partial x_j} - \frac{\nu_j}{x_j^2}(1 - R_j) \right). \quad (6)$$

These operators satisfy a deformed Heisenberg algebra

$$[x_i, D_j] = \delta_{ij}(1 + 2\nu_j R_j), \quad [D_i, D_j] = [x_i, x_j] = 0. \quad (7)$$

2.3 Explicit Form of the Dunkl–Pauli Hamiltonian

Substituting the Dunkl momentum and the AB vector potential into Eq. (1), the Hamiltonian can be organized as [33]

$$\begin{aligned} H = & -\frac{1}{2M}\Delta_D + \frac{1}{2M}\frac{\vartheta^2}{x^2 + y^2} \\ & + \frac{1}{2Mi} \left[\frac{2\vartheta x}{x^2 + y^2} \frac{\partial}{\partial y} - \frac{2\vartheta y}{x^2 + y^2} \frac{\partial}{\partial x} + \frac{2\vartheta x}{x^2 + y^2} \frac{\nu_2}{y}(1 - R_2) - \frac{2\vartheta y}{x^2 + y^2} \frac{\nu_1}{x}(1 - R_1) \right] \\ & + \frac{1}{2M}\sigma_z \left[\frac{2\vartheta}{x^2 + y^2}(\nu_1 R_1 + \nu_2 R_2) - \vartheta \frac{\delta(r)}{r} \right] + \frac{1}{2}M\omega^2(x^2 + y^2). \end{aligned} \quad (8)$$

2.4 Separation in Polar Coordinates

Transforming to polar coordinates (r, φ) with $x = r \cos \varphi$, $y = r \sin \varphi$, the Hamiltonian separates into radial and angular parts

$$H = -\frac{1}{2M}\frac{\partial^2}{\partial r^2} - \frac{1 + 2\nu_1 + 2\nu_2}{2Mr}\frac{\partial}{\partial r} + \frac{1}{2}M\omega^2 r^2 + \frac{1}{Mr^2}\mathcal{H}_\varphi, \quad (9)$$

where the angular operator \mathcal{H}_φ is given by

$$\mathcal{H}_\varphi = \mathcal{B}_\varphi - \vartheta \mathcal{J}_\varphi + \sigma_z \vartheta (\nu_1 R_1 + \nu_2 R_2) - \frac{\vartheta}{2} r \delta(r) \sigma_z. \quad (10)$$

The Dunkl angular operators \mathcal{B}_φ and \mathcal{J}_φ are defined as [31, 32]

$$\mathcal{B}_\varphi = -\frac{1}{2} \frac{\partial^2}{\partial \varphi^2} + (\nu_1 \tan \varphi - \nu_2 \cot \varphi) \frac{\partial}{\partial \varphi} + \frac{\nu_1}{2 \cos^2 \varphi} (1 - R_1) + \frac{\nu_2}{2 \sin^2 \varphi} (1 - R_2), \quad (11)$$

$$\mathcal{J}_\varphi = i \left[\frac{\partial}{\partial \varphi} + \nu_2 \cot \varphi (1 - R_2) - \nu_1 \tan \varphi (1 - R_1) \right], \quad (12)$$

and satisfy the relation

$$\mathcal{J}_\varphi^2 = 2\mathcal{B}_\varphi + 2\nu_1\nu_2(1 - R_1R_2). \quad (13)$$

2.5 Angular Eigenvalue Problem

Since R_1R_2 commutes with \mathcal{J}_φ , we seek factorized solutions of the form

$$\psi(r, \varphi) = R(r) \Phi_\epsilon(\varphi) \chi_{m_s}, \quad (14)$$

where χ_{m_s} are the spin eigenfunctions satisfying $\sigma_z \chi_{m_s} = m_s \chi_{m_s}$ with $m_s = \pm 1$, and $\Phi_\epsilon(\varphi)$ are eigenfunctions of \mathcal{J}_φ :

$$\mathcal{J}_\varphi \Phi_\epsilon(\varphi) = \lambda_\epsilon \Phi_\epsilon(\varphi). \quad (15)$$

The subscript $\epsilon = \epsilon_1 \epsilon_2$ labels the joint reflection eigenvalues, with $R_j \Phi_\epsilon = \epsilon_j \Phi_\epsilon$ and $\epsilon_j = \pm 1$. The explicit form of these eigenfunctions depends on the parity sector [17, 29].

Even sector $\epsilon = +1$ ($\epsilon_1 = \epsilon_2 = \pm 1$):

$$\Phi_+(\varphi) = A_l P_l^{(\nu_1 - \frac{1}{2}, \nu_2 - \frac{1}{2})}(-2 \cos \varphi) \pm i A'_l \sin \varphi \cos \varphi P_{l-1}^{(\nu_1 + \frac{1}{2}, \nu_2 + \frac{1}{2})}(-2 \cos \varphi), \quad (16)$$

$$\lambda_+ = \pm 2 \sqrt{l(l + \nu_1 + \nu_2)}, \quad l \in \mathbb{N}^*, \quad (17)$$

with normalization constants

$$A_l = \sqrt{\frac{(2l + \nu_1 + \nu_2) \Gamma(l + \nu_1 + \nu_2) l!}{2 \Gamma(l + \nu_1 + \frac{1}{2}) \Gamma(l + \nu_2 + \frac{1}{2})}}, \quad \text{and} \quad A'_l = \sqrt{\frac{(2l + \nu_1 + \nu_2) \Gamma(l + \nu_1 + \nu_2 + 1) (l-1)!}{2 \Gamma(l + \nu_1 + 1/2) \Gamma(l + \nu_2 + \frac{1}{2})}}$$

Odd sector $\epsilon = -1$ ($\epsilon_1 = -\epsilon_2$):

$$\Phi_-(\varphi) = B_l \cos \varphi P_{l-\frac{1}{2}}^{(\nu_1 + \frac{1}{2}, \nu_2 - \frac{1}{2})}(-2 \cos \varphi) \mp i B'_l \sin \varphi P_{l-\frac{1}{2}}^{(\nu_1 - \frac{1}{2}, \nu_2 + \frac{1}{2})}(-2 \cos \varphi), \quad (18)$$

$$\lambda_- = \pm 2 \sqrt{(l + \nu_1)(l + \nu_2)}, \quad l \in \left\{ \frac{1}{2}, \frac{3}{2}, \frac{5}{2}, \dots \right\}, \quad (19)$$

with

$$B_l = \sqrt{\frac{(2l + \nu_1 + \nu_2) \Gamma(l + \nu_1 + \nu_2 + 1/2) \Gamma(n - 1/2)!}{2 \Gamma(n + \nu_1 + 1) \Gamma(n + \nu_2)}} \quad \text{and} \quad B'_l = \sqrt{\frac{(2l + \nu_1 + \nu_2) \Gamma(l + \nu_1 + \nu_2 + 1) (l - \frac{1}{2})!}{2 \Gamma(l + \nu_1) \Gamma(l + \nu_2 + 1)}}$$

Here $P_n^{(a,b)}$ denote Jacobi polynomials.

2.6 Radial Equation and Regularization

Inserting the angular eigenfunctions into Eq. (9) and using $\mathcal{Q}(r) = r^{-\delta}\mathcal{L}(r)$ with $\delta = \frac{1}{2} + \nu_1 + \nu_2$, we obtain the radial equation

$$\left[-\frac{d^2}{dr^2} + \frac{(\vartheta - \lambda_\epsilon)^2 + \delta(\delta - 1) - 2\nu_1\nu_2(1 - \epsilon) + 2\vartheta(\nu_1\epsilon_1 + \nu_2\epsilon_2)m_s}{r^2} - \vartheta m_s \frac{\delta(r)}{r} + M^2\omega^2 r^2 \right] \mathcal{L}(r) = 2ME\mathcal{L}(r). \quad (20)$$

The term $\delta(r)/r$ renders the differential operator singular at the origin. Following the self-adjoint extension approach, we regularize by replacing the zero-radius flux tube with a finite one of radius R ,

$$\frac{\delta(r)}{r} \longrightarrow \frac{\delta(r - R)}{r}, \quad e\mathbf{A} = -\frac{\vartheta}{r}\theta(r - R)\mathbf{u}_\varphi, \quad (21)$$

solving the problem for $R > 0$ and then taking the limit $R \rightarrow 0^+$.

Using the identity

$$\delta(\delta - 1) - 2\nu_1\nu_2(1 - \epsilon) = (\nu_1 + \epsilon\nu_2)^2 - \frac{1}{4}, \quad (22)$$

we define the effective angular momenta

$$K_-^2 = \lambda_\epsilon^2 + (\nu_1 + \epsilon\nu_2)^2, \quad (23)$$

$$K_+^2 = (\vartheta - \lambda_\epsilon)^2 + (\nu_1 + \epsilon\nu_2)^2 + 2\vartheta(\nu_1\epsilon_1 + \nu_2\epsilon_2)m_s. \quad (24)$$

The radial equations in the inner ($r < R$) and outer ($r > R$) regions then take the standard oscillator form

$$\left[\frac{d^2}{dr^2} - \frac{K_-^2 - 1/4}{r^2} - M^2\omega^2 r^2 + 2ME_- \right] \mathcal{L}_-(r) = 0, \quad r < R, \quad (25)$$

$$\left[\frac{d^2}{dr^2} - \frac{K_+^2 - 1/4}{r^2} - M^2\omega^2 r^2 + 2ME_+ \right] \mathcal{L}_+(r) = 0, \quad r > R. \quad (26)$$

2.7 Radial Solutions and Matching Conditions

The normalizable solutions of Eqs. (25) and (26) are expressed in terms of generalized Laguerre polynomials

$$\mathcal{L}_-(r) = N_- r^{K_- + 1/2} e^{-M\omega r^2/2} L_n^{K_-}(M\omega r^2), \quad (27)$$

$$\mathcal{L}_+(r) = N_+ r^{K_+ + 1/2} e^{-M\omega r^2/2} L_n^{K_+}(M\omega r^2), \quad (28)$$

with corresponding energies

$$E_- = \omega(2n + K_- + 1), \quad n = 0, 1, 2, \dots \quad (29)$$

$$E_+ = \omega(2n + K_+ + 1), \quad n = 0, 1, 2, \dots \quad (30)$$

The delta-function at $r = R$ imposes two matching conditions: continuity of the wave function and a jump in its derivative,

$$\mathcal{L}_-(R) = \mathcal{L}_+(R), \quad (31)$$

$$\frac{d\mathcal{L}_+}{dr} \Big|_{r=R} - \frac{d\mathcal{L}_-}{dr} \Big|_{r=R} - \frac{\vartheta m_s}{R} \mathcal{L}_-(R) = 0. \quad (32)$$

To leading order in R , the Laguerre polynomials approach unity and their derivatives vanish. Equation (31) then gives $N_+ = N_- R^{K_- - K_+}$, while Eq. (32) yields the crucial relation

$$K_+ = K_- - \vartheta m_s. \quad (33)$$

Combining this with Eq. (24) leads to the constraint

$$\nu_1 \epsilon_1 + \nu_2 \epsilon_2 = \nu_1 + \epsilon \nu_2 = 0, \quad (34)$$

This relation reflects a compatibility condition between the reflection symmetry introduced by the Dunkl operators and the topological phase generated by the Aharonov-Bohm (AB) flux. This constraint arises from the matching conditions imposed by the singular magnetic interaction at the origin and ensures the regularity of the wavefunction in the presence of the flux tube. Physically, it implies that the reflection deformations along the two spatial directions cannot be chosen independently when a singular AB flux is present. Instead, the topology of the punctured plane imposes a symmetry constraint linking the Dunkl parameters to the reflection sector $\varepsilon = R_1 R_2$. In the absence of the AB flux ($\vartheta = 0$), this restriction disappears and the Dunkl parameters remain independent, recovering the usual Dunkl oscillator. Consequently, the relation may be interpreted as a topology–symmetry compatibility condition between the discrete reflection algebra and the AB phase.

For $\varepsilon = +1$, this requires $\nu_1 = -\nu_2$, leading to $\lambda_+/m_s = 2\ell$; for $\varepsilon = -1$, it requires $\nu_1 = \nu_2$, yielding $\lambda_-/m_s = |2(\ell + \nu_1)|$. This condition is a direct consequence of the AB flux and disappears when $\vartheta = 0$, in agreement with recent time-dependent analyses [33].

2.8 Final Spectrum and Wave Functions

With the constraint (34), the effective angular momenta simplify to

$$K_- = \frac{\lambda_\epsilon}{m_s}, \quad K_+ = \frac{\lambda_\epsilon}{m_s} - \vartheta m_s. \quad (35)$$

Since the particle is confined to the region outside the impenetrable solenoid, the wavefunction must vanish at the boundary, restricting the admissible solutions to those regular in the outer domain. The energy spectrum in the outer region, which contains the physical $R \rightarrow 0$ limit, is therefore

$$E_{n,l,m_s} = \omega \left(2n + \frac{\lambda_\epsilon}{m_s} - \vartheta m_s + 1 \right), \quad n = 0, 1, 2, \dots \quad (36)$$

The corresponding radial eigenfunctions are

$$\mathcal{L}_{n,l,m_s}(r) = \mathcal{N}_{n,l} (M\omega)^{(K_++1/2)/2} r^{K_++1/2} e^{-M\omega r^2/2} L_n^{K_+}(M\omega r^2), \quad (37)$$

with normalization $\mathcal{N}_{n,l} = \sqrt{2n!/\Gamma(n + K_+ + 1)}$. The complete stationary wave function is then

$$\psi_{n,l,m_s,\epsilon}(r, \varphi) = \mathcal{L}_{n,l,m_s}(r) \Phi_\epsilon(\varphi) \chi_{m_s}. \quad (38)$$

This exact solution demonstrates how the Dunkl deformation parameters ν_1, ν_2 and the AB flux ϑ jointly influence the energy spectrum through the angular eigenvalues λ_ϵ and the symmetry constraint (34). The spectrum reduces to the standard Pauli oscillator result when $\nu_1 = \nu_2 = 0$ and $\vartheta = 0$, providing a consistent check of our derivation.

3 Thermodynamic Properties

3.1 Partition Function

A unified formulation of all thermodynamic quantities is achievable once the ground-state energy E_0 is specified for the two reflection sectors. The starting point is the canonical partition function,

$$Z(\beta) = \sum_{n,\ell,m_s} e^{-\beta E_{n,\ell,m_s}}, \quad \beta = \frac{1}{k_B T}.$$

The spectra analyzed in Sec. 2 give rise to partition functions that share a common functional form,

$$Z(\beta) = \frac{2 e^{-\beta E_0} \cosh(\beta \omega \vartheta)}{(1 - e^{-2\beta \omega})^2}, \quad (39)$$

where the model-dependent ground-state energy E_0 is given by

$$E_0 = \begin{cases} \omega(1 + 2\ell_0), & \varepsilon = +1, \\ 2\omega(\ell_0 + \nu + \frac{3}{2}), & \varepsilon = -1. \end{cases} \quad (40)$$

Here ℓ_0 denotes the lowest admissible angular quantum number—an integer for $\varepsilon = +1$ and a half-integer offset for $\varepsilon = -1$ —whose value is determined by the regularity conditions $K_{\pm} > -1$, as detailed below.

Determination of ℓ_0

- For $\varepsilon = +1$, the angular quantum number takes integer values, $\ell \in \{1, 2, 3, \dots\}$, subject to the constraint

$$\ell \geq \max\left(1, \left\lceil \frac{\vartheta m_s - 1}{2} \right\rceil\right).$$

Consequently,

$$\ell_0 = \begin{cases} 1, & |\vartheta| \leq 3, \\ \left\lceil \frac{\vartheta m_s - 1}{2} \right\rceil, & |\vartheta| > 3, \end{cases}$$

where $\lceil \cdot \rceil$ denotes the ceiling function (the smallest integer greater than or equal to its argument). To illustrate how the partition function depends on temperature and the AB flux, we plot $Z(T)$ for the $\varepsilon = +1$ sector. The curves show a monotonic increase with temperature, with the flux parameter ϑ controlling the low-temperature offset through its influence on the ground-state energy

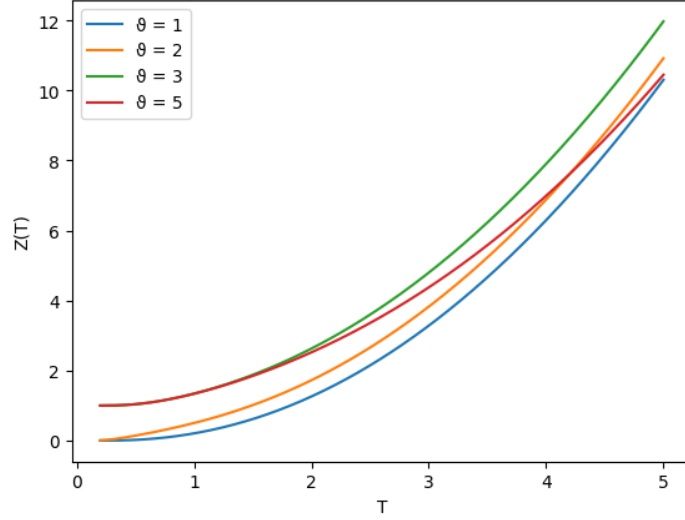


Figure 1: Temperature dependence of $Z(T)$ for $\varepsilon = +1$ and several values of the AB flux ϑ .

- For $\varepsilon = -1$, the angular quantum number is half-integer, $\ell \in \{\frac{1}{2}, \frac{3}{2}, \frac{5}{2}, \dots\}$, and satisfies

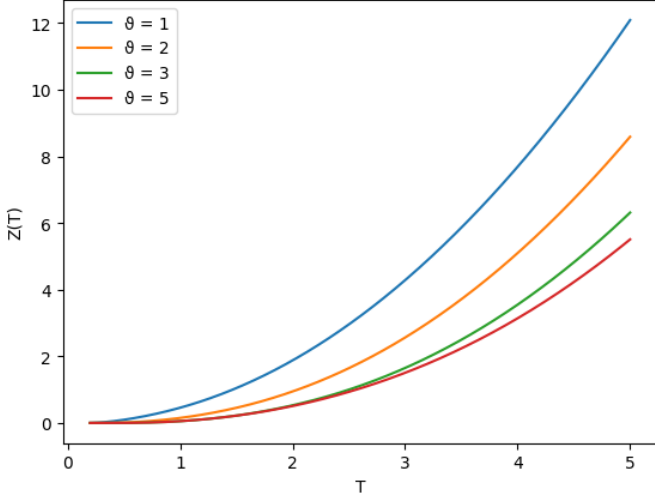
$$\ell \geq \max\left(\frac{1}{2}, \left\lceil \frac{\vartheta m_s - 2\nu - 1}{2} \right\rceil + \frac{1}{2}\right).$$

Thus,

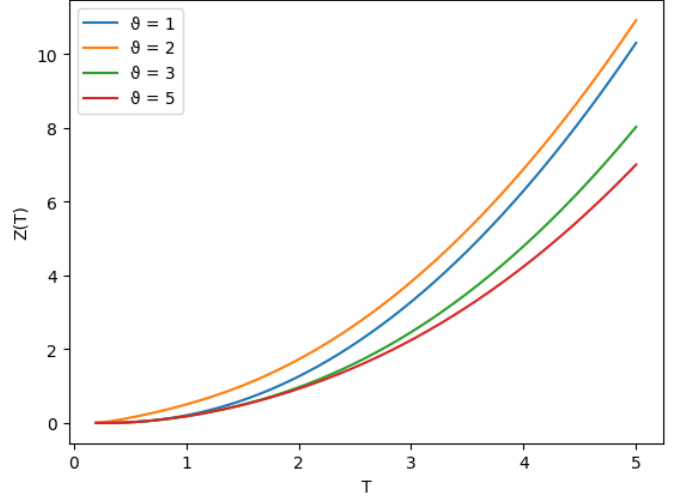
$$\ell_0 = \begin{cases} 0, & |\vartheta| \leq 2(1 + \nu), \\ \left\lceil \frac{\vartheta m_s - 2\nu - 1}{2} \right\rceil, & |\vartheta| > 2(1 + \nu), \end{cases}$$

and the actual lowest half-integer angular momentum is $\ell = \ell_0 + \frac{1}{2}$.

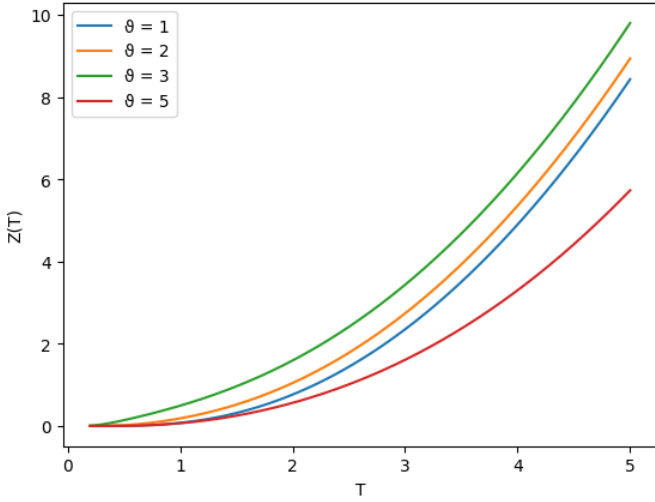
For the $\varepsilon = -1$ sector, the partition function acquires an additional dependence on the Dunkl parameter ν . Figure 2 displays $Z(T)$ for various combinations of ν and ϑ , revealing how the deformation parameter modulates the thermal response of the system. The four panels correspond to different values of ν , allowing a direct comparison of the Dunkl deformation effects.



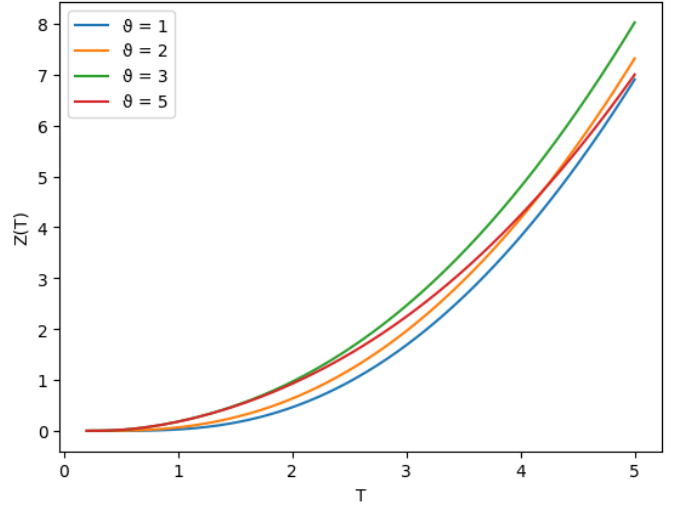
(a) Partition Function $Z(T)$, $\varepsilon = -1$, $\vartheta = -0.4$



(b) Partition Function $Z(T)$, $\varepsilon = -1$, $\vartheta = 0.0$



(c) Partition Function $Z(T)$, $\varepsilon = -1$, $\vartheta = 0.5$



(d) Partition Function $Z(T)$, $\varepsilon = -1$, $\vartheta = 1.0$

Figure 2: Temperature dependence of $Z(T)$ for $\varepsilon = -1$ and several values of the Dunkl parameter ν and the AB flux ϑ .

3.2 Internal Energy.

From $U = -\partial_\beta \ln Z$ (with $\partial_\beta \equiv \partial/\partial\beta$), one obtains

$$U(\beta) = E_0 - \omega\vartheta \tanh(\beta\omega\vartheta) - \frac{4\omega}{e^{2\beta\omega} - 1}. \quad (41)$$

The temperature dependence of the internal energy for the $\varepsilon = +1$ sector is shown in Figure 3. At low temperatures, $U(T)$ approaches the ground-state energy E_0 , which increases with $|\vartheta|$. As temperature rises, all curves converge toward the classical equipartition limit, with the flux-induced splitting persisting only at intermediate temperatures.

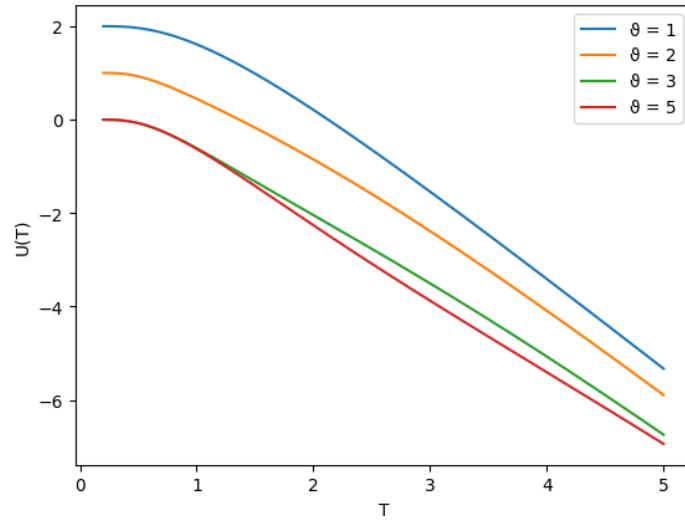
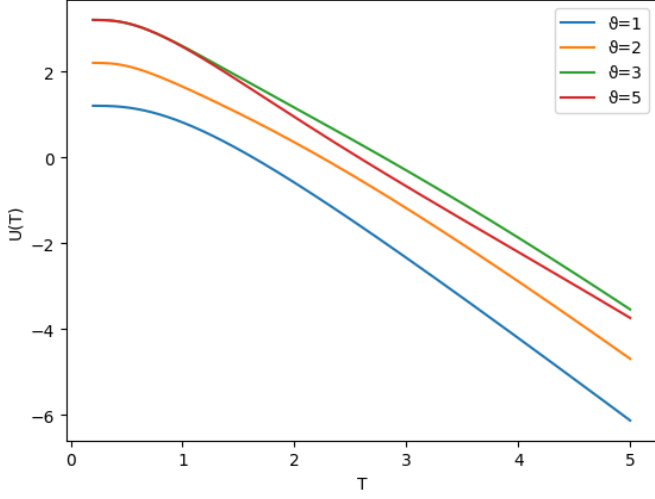
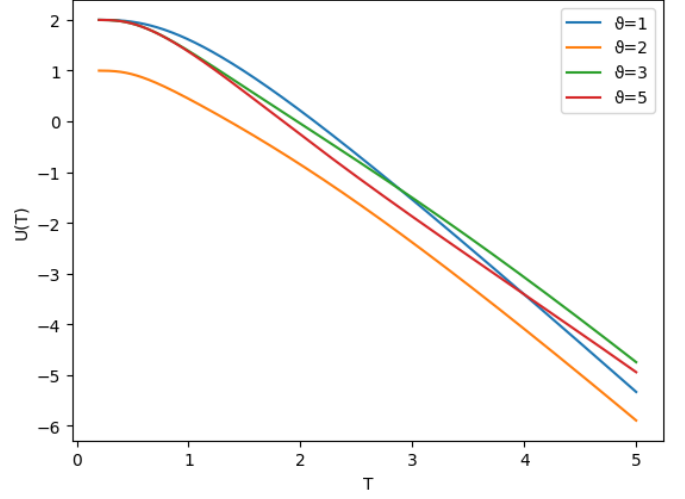


Figure 3: Temperature dependence of internal energy $U(T)$ for $\varepsilon = +1$ and several values of the AB flux ϑ .

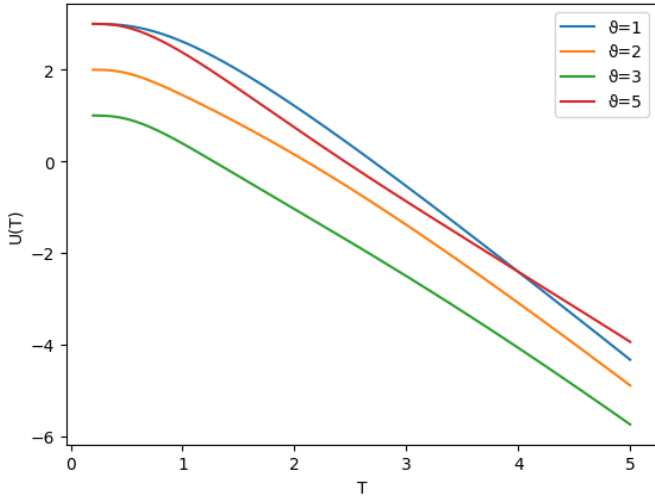
For $\varepsilon = -1$, the internal energy exhibits a richer structure due to the interplay between the Dunkl parameter ν and the AB flux ϑ . Figure 4 presents $U(T)$ for four representative values of ν , each panel showing multiple flux values. The deformation parameter ν systematically shifts the energy scale, with larger ν leading to higher ground-state energies and more pronounced thermal activation.



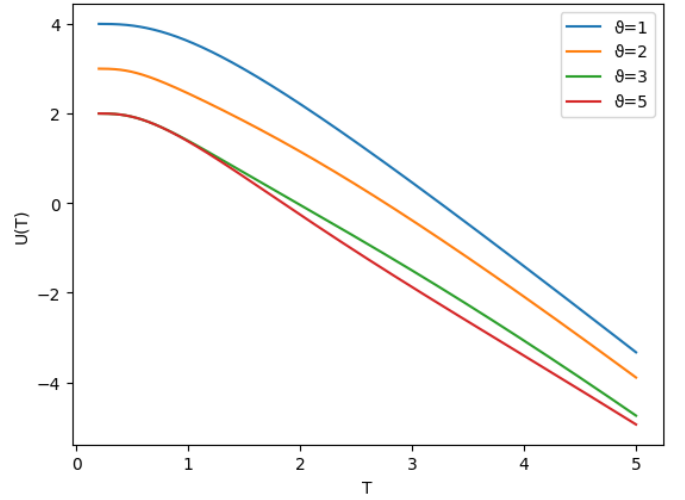
(a) Internal Energy $U(T)$, $\varepsilon = -1$, $\vartheta = -0.4$



(b) Internal Energy $U(T)$, $\varepsilon = -1$, $\vartheta = 0.0$



(c) Internal Energy $U(T)$, $\varepsilon = -1$, $\vartheta = 0.5$



(d) Internal Energy $U(T)$, $\varepsilon = -1$, $\vartheta = 1.0$

Figure 4: Temperature dependence of internal energy $U(T)$ for $\varepsilon = -1$ and several values of the Dunkl parameter ν and the AB flux ϑ .

3.3 Entropy.

The entropy follows from $S = \beta(U - F)$. Substituting the above expressions yields

$$\begin{aligned}
 S(\beta) = & \ln[2 \cosh(\beta\omega\vartheta)] - 2 \ln(1 - e^{-2\beta\omega}) \\
 & - \beta\omega\vartheta \tanh(\beta\omega\vartheta) - \frac{4\beta\omega}{e^{2\beta\omega} - 1}.
 \end{aligned} \tag{42}$$

To restore the explicit Boltzmann constant, replace $S \rightarrow k_B S$ and $\beta \rightarrow 1/(k_B T)$.

The entropy is identical for both $\varepsilon = \pm 1$ sectors, vanishes at low temperatures, and its thermal activation is delayed by larger AB flux ϑ , with no dependence on the Dunkl parameter ν .

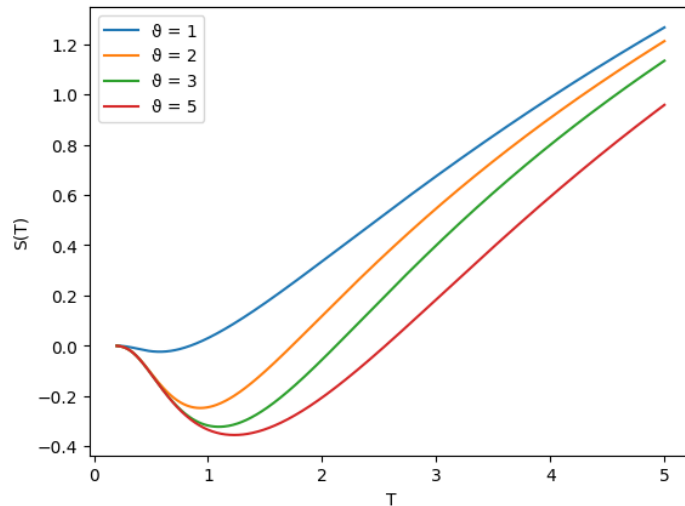


Figure 5: Temperature dependence of $S(T)$ for several values of the AB flux ϑ .

3.4 Heat Capacity.

Differentiating (41) and using $C_V = \partial U / \partial T = -\beta^2 \partial_\beta U$ gives

$$C_V(\beta) = \beta^2 \omega^2 \left[\vartheta^2 \operatorname{sech}^2(\beta \omega \vartheta) + 2 \operatorname{csch}^2(\beta \omega) \right]. \quad (43)$$

The heat capacity exhibits a Schottky peak whose position and amplitude are controlled by the AB flux ϑ , with larger fluxes shifting the peak to higher temperatures while reducing its height, before all curves approach the classical Dulong–Petit limit $C_V = 2$ at high temperatures.

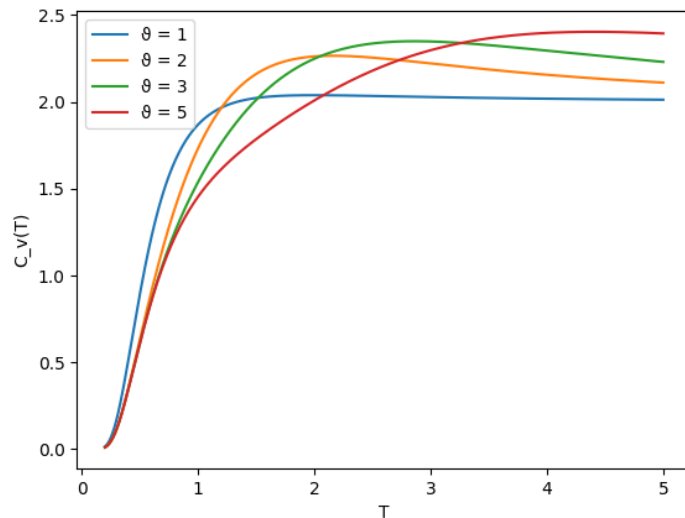


Figure 6: Heat Capacity $C_V(T)$ for several values of the AB flux ϑ .

3.5 Results and Discussion

The thermodynamic behavior of the Dunkl–Pauli oscillator in the presence of an Aharonov–Bohm (AB) flux can be analyzed through the temperature dependence of the partition function, Helmholtz free energy, internal energy, entropy, and heat capacity. The numerical results obtained from the analytical

expressions derived above are illustrated in Figs. 1–8 for different values of the AB flux ϑ and the Dunkl parameter ν , and for the two reflection sectors $\varepsilon = \pm 1$.

Figures 1 and 2 show the temperature dependence of the partition function $Z(T)$ for the two reflection sectors. In both cases, the partition function increases monotonically with temperature, reflecting the progressive thermal population of higher-energy states. For the sector $\varepsilon = +1$ (Fig. 1), increasing the AB flux ϑ enhances the value of the partition function, indicating that the magnetic flux modifies the density of accessible quantum states through its influence on the energy spectrum. In the sector $\varepsilon = -1$ (Fig. 2), the partition function depends additionally on the Dunkl parameter ν , which modifies the effective centrifugal contribution appearing in the radial Hamiltonian. Consequently, the combined effects of reflection symmetry and magnetic flux lead to noticeable shifts in the thermal curves.

Figures 3 and 4 illustrate the temperature dependence of the internal energy $U(T)$. At very low temperatures, the internal energy approaches the ground-state value, as thermal excitations are strongly suppressed. As the temperature increases, $U(T)$ grows smoothly due to the increasing occupation of excited oscillator states. The presence of the AB flux produces a shift in the internal energy curves, reflecting the influence of the topological phase on the quantization of angular momentum and therefore on the energy spectrum. In the $\varepsilon = -1$ sector, the Dunkl parameter introduces additional variations in the internal energy, highlighting the role of reflection symmetry in the thermodynamic properties of the system.

The entropy $S(T)$, shown in Fig. 5, increases monotonically with temperature. In the low-temperature regime the entropy tends toward zero, which is consistent with the third law of thermodynamics since the system occupies its ground state. As the temperature rises, more quantum states become thermally accessible and the entropy increases smoothly. The AB flux slightly modifies the entropy curves by shifting the underlying energy spectrum.

The heat capacity $C_V(T)$ displayed in Fig. 6 exhibits a rapid increase at low temperatures, corresponding to the onset of thermal excitations. At higher temperatures it gradually approaches a constant value, consistent with the equipartition theorem for a system with two quadratic degrees of freedom. In this regime the influence of the AB flux becomes less pronounced because the thermal energy dominates over the quantum corrections introduced by the topological phase.

Further insight into the thermodynamic properties can be obtained by considering the limiting temperature regimes.

Low-temperature limit ($T \rightarrow 0$). In the limit $\beta \rightarrow \infty$, the exponential factors suppress all excited states and the partition function is dominated by the ground state,

$$Z(\beta) \sim e^{-\beta E_0}.$$

The internal energy approaches

$$U \rightarrow E_0 - \omega\vartheta \operatorname{sgn}(\vartheta),$$

while the entropy tends to zero,

$$S \rightarrow 0,$$

in agreement with the third law of thermodynamics. In this regime the heat capacity also vanishes,

$$C_V \rightarrow 0,$$

indicating that thermal fluctuations are strongly suppressed and the system remains essentially in its ground state.

High-temperature limit ($T \rightarrow \infty$). In the opposite limit $\beta \rightarrow 0$, the hyperbolic functions can be expanded as

$$\cosh(\beta\omega\vartheta) \approx 1, \quad \sinh(\beta\omega) \approx \beta\omega.$$

The partition function then behaves as

$$Z(\beta) \sim \frac{1}{2(\beta\omega)^2},$$

showing that the thermal behavior is dominated by the oscillator degrees of freedom. The internal energy approaches

$$U \approx 2k_B T,$$

which agrees with the equipartition theorem for two quadratic degrees of freedom. Consequently, the heat capacity tends to the constant value

$$C_V \rightarrow 2k_B,$$

indicating that the influence of the Aharonov–Bohm flux becomes negligible at sufficiently high temperatures.

Overall, these results demonstrate that the thermodynamic behavior of the Dunkl–Pauli oscillator is governed by the interplay between the reflection symmetry introduced by the Dunkl operators and the topological phase associated with the AB flux. While the AB flux and the Dunkl deformation significantly modify the spectrum and thermodynamic quantities at low temperatures, their influence gradually diminishes in the high-temperature regime where the system approaches the behavior of a standard two-dimensional harmonic oscillator.

4 Conclusion

In this work, we studied the Dunkl–deformed Pauli oscillator in two dimensions in the presence of an Aharonov–Bohm (AB) flux. The incorporation of Dunkl operators introduces reflection symmetry into the Pauli Hamiltonian, while the magnetic flux produces a topological phase that modifies the quantization of angular momentum.

By solving the corresponding eigenvalue problem, the exact energy spectrum of the system was obtained. The reflection symmetry leads to two distinct sectors characterized by $\varepsilon = \pm 1$, each associated with specific constraints on the Dunkl parameters and on the allowed values of the angular quantum number. As a consequence, the energy levels depend explicitly on both the reflection symmetry and the AB flux parameter.

Using the derived spectrum, the canonical partition function was constructed and expressed in a unified analytical form. This formulation allowed the calculation of the main thermodynamic quantities, including the Helmholtz free energy, internal energy, entropy, and heat capacity. The results show that the magnetic flux modifies the ground-state energy through the lowest admissible angular momentum ℓ_0 , which directly affects the thermodynamic behavior of the system.

The analysis further indicates that the influence of the AB flux is significant in the low-temperature regime, where the ground state dominates the partition function, whereas at high temperatures the thermodynamic quantities approach the standard oscillator limit. These results demonstrate that the combined effects of reflection symmetry and topological gauge phases lead to characteristic modifications of the spectral and thermodynamic properties of the Dunkl–Pauli oscillator.

References

- [1] J. M. Leinaas and J. Myrheim, On the theory of identical particles, *Il Nuovo Cimento B* **37**, 1–23 (1977). <https://doi.org/10.1007/BF02727953>.

- [2] F. Wilczek, Quantum mechanics of fractional-spin particles, *Phys. Rev. Lett.* **49**, 957–959 (1982). <https://doi.org/10.1103/PhysRevLett.49.957>.
- [3] Y. Aharonov and D. Bohm, Significance of electromagnetic potentials in the quantum theory, *Phys. Rev.* **115**, 485–491 (1959). <https://doi.org/10.1103/PhysRev.115.485>.
- [4] Y. Aharonov and D. Bohm, Further considerations on electromagnetic potentials in the quantum theory, *Phys. Rev.* **123**, 1511–1524 (1961). <https://doi.org/10.1103/PhysRev.123.1511>.
- [5] S. Olariu and I. I. Popescu, The quantum effects of electromagnetic fluxes, *Rev. Mod. Phys.* **57**, 339–436 (1985). <https://doi.org/10.1103/RevModPhys.57.339>.
- [6] M. Peshkin and A. Tonomura, *The Aharonov-Bohm Effect*, Springer (1989). <https://doi.org/10.1007/BFb0032076>.
- [7] R. G. Chambers, Shift of an electron interference pattern by enclosed magnetic flux, *Phys. Rev. Lett.* **5**, 3–5 (1960). <https://doi.org/10.1103/PhysRevLett.5.3>.
- [8] A. Tonomura et al., Evidence for Aharonov–Bohm effect with magnetic field completely shielded from electron wave, *Phys. Rev. Lett.* **56**, 792–795 (1986). <https://doi.org/10.1103/PhysRevLett.56.792>.
- [9] M. V. Berry, Quantal phase factors accompanying adiabatic changes, *Proc. R. Soc. Lond. A* **392**, 45–57 (1984). <https://doi.org/10.1098/rspa.1984.0023>.
- [10] W. Pauli, Zur Quantenmechanik des magnetischen Elektrons, *Z. Physik* **43**, 601–623 (1927). <https://doi.org/10.1007/BF01397326>.
- [11] P. A. M. Dirac, The quantum theory of the electron, *Proc. R. Soc. Lond. A* **117**, 610–624 (1928). <https://doi.org/10.1098/rspa.1928.0023>.
- [12] C. R. Hagen, Exact equivalence of spin-1/2 Aharonov-Bohm and Aharonov-Casher effects, *Phys. Rev. Lett.* **64**, 2347 (1990). <https://doi.org/10.1103/PhysRevLett.64.2347>.
- [13] K. von Klitzing, G. Dorda, and M. Pepper, New method for high-accuracy determination of the fine-structure constant based on quantized Hall resistance, *Phys. Rev. Lett.* **45**, 494–497 (1980). <https://doi.org/10.1103/PhysRevLett.45.494>.
- [14] D. C. Tsui, H. L. Stormer, and A. C. Gossard, Two-dimensional magnetotransport in the extreme quantum limit, *Phys. Rev. Lett.* **48**, 1559–1562 (1982). <https://doi.org/10.1103/PhysRevLett.48.1559>.
- [15] C. W. J. Beenakker, Colloquium: Andreev reflection and Klein tunneling in graphene, *Rev. Mod. Phys.* **80**, 1337–1354 (2008). <https://doi.org/10.1103/RevModPhys.80.1337>.
- [16] Y. Bouguerra, A. Bounames, M. Maamache, and Y. Saadi, Time-dependent Pauli equation in the presence of the Aharonov–Bohm effect, *J. Math. Phys.* **49**, 042107 (2008). <https://doi.org/10.1063/1.2903752>.
- [17] H. Bouguerne, B. Hamil, B. C. Lütüoğlu, and M. Merad, Dunkl–Pauli equation in the presence of a magnetic field, *Indian J. Phys.* **98**, 4093–4105 (2024). <https://doi.org/10.1007/s12648-024-03170-y>.
- [18] C. F. Dunkl, Differential-difference operators associated to reflection groups, *Trans. Amer. Math. Soc.* **311**, 167–183 (1989). <https://doi.org/10.1090/S0002-9947-1989-0951883-8>.

- [19] C. F. Dunkl, Integral kernels with reflection group invariance, *Canad. J. Math.* **43**, 1213–1227 (1991). <https://doi.org/10.4153/CJM-1991-069-8>.
- [20] M. Rösler, Dunkl operators: Theory and applications, In *Orthogonal Polynomials and Special Functions*, Springer, pp. 93–135 (2003). <https://doi.org/10.1007/b12166>.
- [21] C. F. Dunkl, Reflection groups in analysis and applications, *Jpn. J. Math.* **3**, 215–246 (2008). <https://doi.org/10.1007/s11537-008-0819-3>.
- [22] C. F. Dunkl and Y. Xu, *Orthogonal Polynomials of Several Variables*, 2nd ed., Cambridge University Press (2014). <https://doi.org/10.1017/CBO9781107786134>.
- [23] F. Calogero, Solution of the one-dimensional N-body problems with quadratic and/or inversely quadratic pair potentials, *J. Math. Phys.* **12**, 419–436 (1971). <https://doi.org/10.1063/1.1665604>.
- [24] B. Sutherland, Exact results for a quantum many-body problem in one dimension, *Phys. Rev. A* **4**, 2019–2021 (1971). [10.1103/PhysRevA.4.2019](https://doi.org/10.1103/PhysRevA.4.2019)
- [25] J. Moser, Three integrable Hamiltonian systems connected with isospectral deformations, *Adv. Math.* **16**, 197–220 (1975). [10.1016/0001-8708\(75\)90151-6](https://doi.org/10.1016/0001-8708(75)90151-6)
- [26] M. A. Olshanetsky and A. M. Perelomov, Classical integrable finite-dimensional systems related to Lie algebras, *Phys. Rep.* **71**, 313–400 (1981). [10.1016/0370-1573\(81\)90023-5](https://doi.org/10.1016/0370-1573(81)90023-5)
- [27] R. D. Mota, D. Ojeda-Guillén, M. Salazar-Ramírez, and V. D. Granados, Landau levels for the $(2 + 1)$ Dunkl–Klein–Gordon oscillator, *Mod. Phys. Lett. A* **36**, 2150066 (2021). [10.1142/S0217732321500668](https://doi.org/10.1142/S0217732321500668)
- [28] R. D. Mota, D. Ojeda-Guillén, M. Salazar-Ramírez, and V. D. Granados, Exact solutions of the 2D Dunkl–Klein–Gordon equation: The Coulomb potential and the Klein–Gordon oscillator, *Mod. Phys. Lett. A* **36**, 2150171 (2021). [10.1142/S0217732321501716](https://doi.org/10.1142/S0217732321501716)
- [29] A. Benchikha, B. Hamil, and B. C. Lütfüoğlu, Time-dependent Dunkl–Pauli oscillator, *Indian J. Phys.* **99**, 4677–4686 (2025). [10.1007/s12648-025-03637-6](https://doi.org/10.1007/s12648-025-03637-6)
- [30] S. Hassanabadi, P. Sedaghatnia, W. S. Chung, et al., Exact solution to two dimensional Dunkl harmonic oscillator in the non-commutative phase-space, *Eur. Phys. J. Plus* **138**, 331 (2023). [10.1140/epjp/s13360-023-03933-2](https://doi.org/10.1140/epjp/s13360-023-03933-2)
- [31] V. X. Genest, M. E. H. Ismail, L. Vinet, and A. Zhedanov, The Dunkl oscillator in the plane: I. Superintegrability, separated wavefunctions and overlap coefficients, *J. Phys. A: Math. Theor.* **46**, 145201 (2013). [10.1088/1751-8113/46/14/145201](https://doi.org/10.1088/1751-8113/46/14/145201)
- [32] V. X. Genest, L. Vinet, and A. Zhedanov, The singular and the 2:1 anisotropic Dunkl oscillators in the plane, *J. Phys. A: Math. Theor.* **46**, 325201 (2013). [10.1088/1751-8113/46/32/325201](https://doi.org/10.1088/1751-8113/46/32/325201)
- [33] Boubakeur Khantoul and Ahmed Tedjani Time-dependent Dunkl–Pauli oscillator in the presence of the Aharonov–Bohm effect, *Phys. Scr.* **101**, 085204 (2026). [10.1088/1402-4896/adb123](https://doi.org/10.1088/1402-4896/adb123)